Numerical Simulations of Gas Burner Experiments in a Residential Structure with HVAC System

Dushyant M. Chaudhari ⓘ*, *Craig Weinschenk* ⓘ *and Jason E. Floyd* ⓘ, *Fire Safety Research Institute, UL Research Institutes, 6200 Old Dobbin Lane, Suite 150, Columbia, MD 21045, USA*

Abstract. Controlled fire experiments using a gas burner were previously conducted in a purpose-built, two-story, moderately air-tight residential structure to understand the effect of a heating, ventilating, and air conditioning (HVAC) system and door positions on the fire-induced environment. Temperatures, gas concentrations (oxygen, water vapor, carbon dioxide), and differential pressures were monitored throughout the structure. HVAC status (off vs. on) and stairwell door position of the fire room (open vs. closed) were varied for the experiments analyzed in this paper. In this study, Fire Dynamics Simulator (FDS) v. 6.7.9 was used to simulate these experiments. Experimental data quantifying the air tightness of the building and cold flow-rates through HVAC vents were determined to be important to optimize leakages and HVAC loss coefficients for the simulation setup. Pressure development in the structure was predicted correctly to be higher on the first floor and lower in the basement, but the magnitude of steady-state pressure was underpredicted. The measured and predicted steady-state temperature distributions were statistically different for the cases with and without the HVAC on, regardless of the door position. FDS predicted gas transport through the HVAC duct network, and under-predicted temperature rise and water vapor content by about 9% and 10%, respectively, and over-predicted volumetric oxygen and carbon dioxide content by about 21% and 6%, respectively. Temperature rise prediction in the closed room, where the gas transport primarily occurred via the HVAC duct network, improved after including heat loss from the HVAC duct to the ambient.

Keywords: Gas burner, FDS, Gas transport, Compartment fires

1. Introduction

From 2017 to 2019, the U.S. Fire Administration found that smoke inhalation alone was responsible for more fire-related deaths than thermal burns [1]. The heating, ventilating, and air conditioning (HVAC) system used to maintain local

---

*Correspondence should be addressed to: Dushyant M. Chaudhari, E-mail: dushyant.chaudhari@ul.org

Craig Weinschenk and Jason E. Floyd have contributed equally to this work.

climate of the built environment, can impact the transport of smoke and hot combustion products between compartments.

Previous experiments conducted in compartment-fire settings, with a fire size ranging from 300 kW to 800 kW, investigated the impact of air-tightness of the building and presence of an HVAC system on fire-induced pressure [2, 3] and combustion product transport [4]. Hostikka et al. [2] found that increasing air-tightness of the built environment increases peak overpressure and the visible amount of soot in neighboring compartments and reduces the visibility inside the environment, while open HVAC ducts act as leak paths (if no dampers are used) for mass transport to other parts of the built environment connected to the fire room. A more detailed analysis was performed by Ghanekar et al. [4] where effects of HVAC on combustion product transport were studied by analyzing data obtained from 18 experiments conducted in a purpose-built residential structure. That study presented quantitative evidence that closed doors provided an effective ventilation barrier against the transport of combustion products, regardless of the status of the HVAC system.

Modeling gas transport through an HVAC system is increasingly sought by building designers and fire safety engineers to support performance based design solutions [2, 3, 5–8]. Simulating flow through HVAC ducts using a CFD solver would require finer computational grid in the ducts to resolve flow losses adequately. This can be computationally expensive and therefore, modelers have historically either ignored HVAC systems or modeled them with fixed supply and exhaust rates at HVAC connections to the compartments which does not allow for mass transport between the compartments [6, 7].

In 2011, a solution to this complexity was proposed [6] by coupling a network HVAC model based on MELCOR [9], a thermal hydraulic solver developed to simulate post-accident conditions in a nuclear power plant containment building, with Fire Dynamics Simulator (FDS), a CFD-based model to simulate fire-driven fluid flow which is used for research and fire protection consulting. The model verification involved the study of flow losses and mass and species conservation. The model was validated from experiments involving simple duct network as well as a multi-compartment confined facility with fire. Although this initial coupling methodology provided reasonable results in predicting flow induced by the HVAC system, the initial network model lacked mass storage and heat exchange within the duct network and therefore it could not account for the transport delay of energy and species in a duct (i.e., the time it takes for gases to transit the length of a duct).

In 2019, Ralph et al. [8] developed an approach to model unsteady transport of mass and energy within ducts using the FDS HVAC sub-model. General verification cases involved the study of numerical convergence, species transport time, mass conservation, branching and merging of ducts, energy conservation and pressure. This upgrade to the previous network HVAC model meant that delays in the transport of energy and species through a duct could be modeled; however, at this time the HVAC model as implemented in FDS v. 6.7.9 does not directly simulate heat loss from the ducts, which could lead to overestimation of temperature in HVAC-connected compartments.

Some of the experiments, conducted as a part of the OECD PRISME project in 2013, focused on ventilation effects in compartments typical to a nuclear power plant [10]. These experiments were important for validation of hybrid HVAC modelling framework in FDS, wherein the mechanical ventilation from a tightly sealed fire room was simulated to predict fire-induced pressure with reasonable accuracy [11]. However, further validation of the coupled-hybrid modelling approach for the HVAC model used in FDS is necessary at a full-scale of a residential structure. Experiments conducted by Ghanekar et al. [4] in a purpose-built residential structure are good target experiments to perform this FDS validation exercise. Quiat [12] developed a preliminary FDS model for these experiments but did not evaluate the impact of ventilation on the fire-induced environment.

The purpose of this study was to provide further validation of FDS and the coupled-hybrid modeling approach for simulating the HVAC system. Simulations of the full-scale experiments conducted in the purpose-built residential structure were conducted to understand the capability and discuss the challenges of the current FDS model to predict fire dynamics in a built environment. It is important to note that the fire size used in the full-scale experiments are representative of a developing fire and not a fully developed compartment fire.

2. Experimental Setup

Experiments were conducted in a purpose-built two-story residential structure located at the Delaware County Emergency Services Training Center in Sharon Hill, PA. A total of 29 experiments were conducted using a gas burner located in a bedroom on the first-floor, living-room, or basement with variations in HVAC status and stairwell door positions. A subset of four basement experiments were selected for this study. The basement location was selected because these four experiments were most appropriate to study buoyancy-driven flow to the first-floor and gas transport through the HVAC duct network. The four experiments, listed in Table 1, were all permutations of HVAC status of either 'off' (passive-ducts were open for transport) or 'on' (Cooling with a set temperature of 65° F) and stairwell door status of either closed or open. A brief description of the experimental structure, instrumentation, and the HVAC system relevent to this study is discussed below and detailed information can be found in Ref. [13].

The burner used in the experiments had surface area of 0.65 m$\times$ 0.65 m and was placed in the basement. The top surface of the burner was approximately 0.50 m above the floor for all experiments. The burner fuel was commercial grade propane which was assumed to be comprised of 92.5 vol.% propane, 5 vol.% propylene, and 2.5 vol.% butane. The heat release rate (HRR) of the burner was nominally 300 kW for the basement fires. The expanded uncertainty in the HRR for the burner was estimated to be about $\pm 10\%$ at 300 kW [4]. The experimental structure and a snapshot of a burner flame is shown in Fig. 1.

The floor-plan of the basement and the first-floor, overlaid with the HVAC duct network and instrument locations, is shown in Fig. 2. The first floor of this residential structure had three bedrooms, a living-room, a dining-room, and a

Table 1
Matrix of 4 Experiments Discussed in this Study

Label	Fire-room	HRR (kW)[a]	HVAC status[b]	Stairwell door status	Exp. #[c]
Ba1	Basement	300	Off	Open	23
Ba2	Basement	300	On	Open	24
Ba3	Basement	300	Off	Closed	25
Ba4	Basement	300	On	Closed	26

[a]During the experiments, this was estimated by assuming 100% propane fuel having heat of combustion of 46.4 MJ kg^{-1}

[b]HVAC status 'On' indicate that the cooling was on with a set temperature of 65° F, and 'Off' indicate the passive state of the system

[c]Experiment numbers indicate experiment numbers used for the entire experimental series of 29 experiments

Figure 1. Left: Picture of the purpose-built residential structure. Right: Instance of a gas burner flame from one of the basement fire experiments.

kitchen. The interior dimensions of the first-floor were 13.77 m × 7.68 m × 2.44 m. The basement featured an open-floor plan with interior dimensions of 13.30 m × 7.28 m × 2.74 m. The basement's outer wall was composed of 0.6 m × 0.6 m × 1.2 m interlocking concrete blocks which acted as insulation to emulate a below ground basement. The interior walls of the basement and the first floor were constructed from dimensional lumber, and were covered with 0.013 m thick drywall. The exterior walls of the first-floor were constructed from dimensional lumber and covered with cement board on the outside and 0.013 m thick drywall on the inside. Details of wall components are discussed later in Sect. 3.

2.1. Instrumentation

Measurements acquired during the experiments included temperature, pressure, and gas concentrations of oxygen (O_2), carbon dioxide (CO_2), and water vapor (H_2O). Thermocouple (TC) arrays were used to measure temperature from 0.3 m above the floor at 0.3 m intervals until 0.0254 m below the ceiling in each room/section, as shown by the grey triangles in Fig. 2. All thermocouples in the

TC array were bare-bead, K-type thermocouples with a 1.3 mm bead diameter. Bare-bead thermocouples having similar bead diameter were found to have an associated $\sim \pm 5\%$ error for measurement of temperature below 400°C [14]. Differential pressure was monitored using pressure taps, extending about 0.15 m from the walls, at 0.3 m, 1.22 m, and 2.13 m above the floor at various locations, as shown by orange pentagons in Fig 2. The expanded uncertainty for pressure taps was about 20%. Gas concentrations were obtained at 1.22 m above the floor at locations shown by the blue circles in Fig. 2. For the O_2 and CO_2 concentrations the gas sample was cooled, filtered and passed through a drying agent before being measured using Siemens OxyMat-6 paramagnetic oxygen sensors and Siemens ULTRAMAT-23 non-dispersive infrared (NDIR) gas analyzers, respectively. For the sampling range of 0% to 25% for O_2 and CO_2 sensors, the measured data had an estimated uncertainty of $\pm 12\%$. Measurements of H_2O at the same locations were performed by using an infrared tunable diode laser absorption spectroscopy (IR-TDLAS) based sensor. The relative error, estimated as the standard error of the mean, accounting for temperature uncertainty for H_2O measurement was less than 3% [4].

All data were collected at a 1 Hz sampling frequency during the experiment. At least 120 s of baseline data was collected prior to the ignition of the burner. The fuel supply to the burner was terminated either when the the HVAC filter clogged due to accumulation of soot or when the oxygen concentration near the burner reached 11.5% (lower flammability limit of propane) to ensure safe operation. In all these experiments, bedroom 3 door was always closed and bedroom 2 door was always open.

2.2. HVAC System

The HVAC system included a 10.55 kW cooling capacity and a blower with a volumetric air flowrate capacity of up to 2040 m^3 h^{-1}. The installed system did not have an external supply of fresh air from outside. This system was typical to the Pennsylvania region where the experiments were conducted. The HVAC duct network, made of galvanized steel, was split into a supply and return network. The supply network originated from the top of the furnace unit, which was placed in the mechanical room in the basement. The main basement supply duct measured 0.36 m × 0.20 m. Eight circular ducts, each with 0.18 m diameter, branched off the main duct until the supply vents. These supply vents are labelled with a prefix 'S' (from S-01 through S-08) in Fig. 2. Supply vents in the basement had a cross sectional (C/S) area of 0.238 m × 0.238 m, except for S-06 and S-07 which had a C/S area of 0.279 m × 0.279 m.

A single rectangular duct, with a C/S area of 0.406 m × 0.406 m, ran from the basement to the attic. This duct split into ducts having a C/S area of 0.305 m × 0.305 m which fed the two sides (B and D) of the first floor. All supply vents on the first floor, S-09 through S-16 had a C/S area of 0.305 m × 0.152 m.

The return network originated from the return vents and terminated in the basement mechanical room. Each return vent fed into a plenum space which was comprised of either a floor joist space or a wall stud space. There were five return
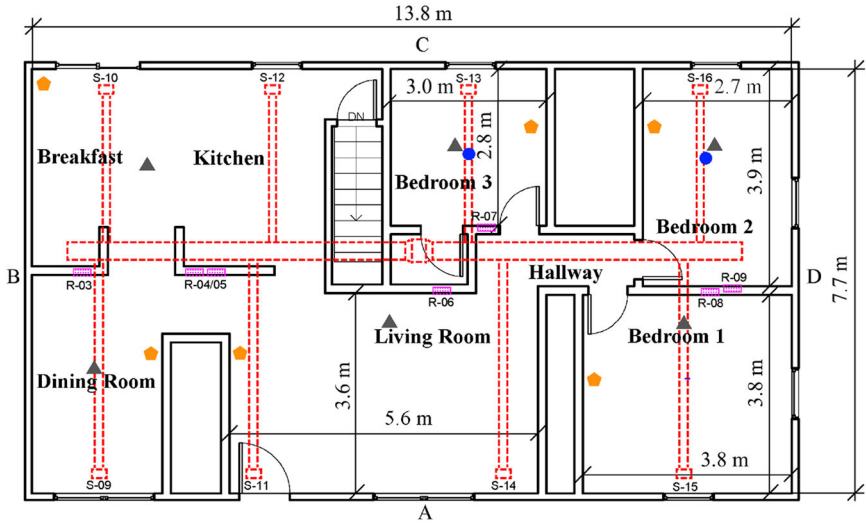
(a) First floor layout
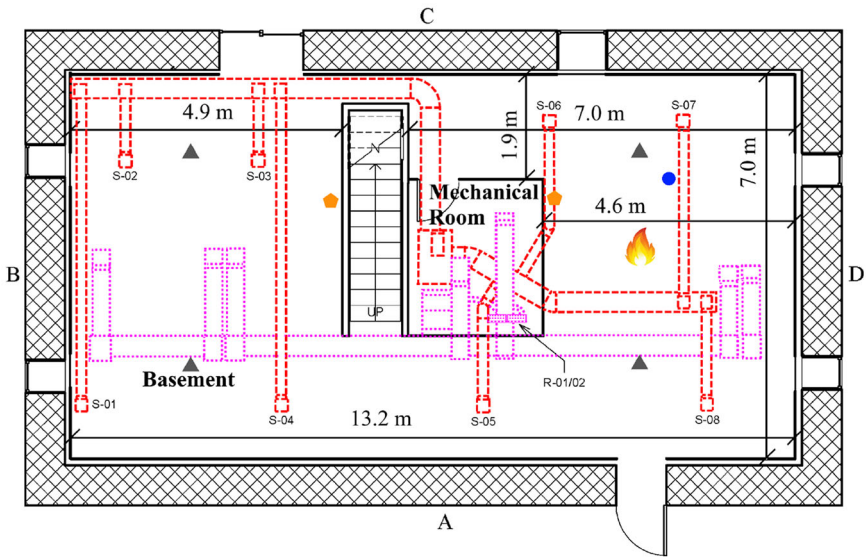
(b) Basement layout

Symbol	Description	Symbol	Description	Symbol	Description
(orange pentagon)	Pressure taps	(gray triangle)	Thermocouple tree	(blue circle)	Gas Sensor

Figure 2. Layout of (a) First Floor, and (b) Basement overlaid with HVAC duct network (Supply network shown in red, and the return network shown in pink) (Color figure online).

vents with C/S area 0.356 m × 0.254 m, that fed into unique joist spaces. Two vents, called 'double returns', with C/S area 0.66 m × 0.254 m, that fed into unique joist spaces. The return vents R-01/02 in the basement and R-04/05 on the first floor in the living-dining room hallway were the two double returns. The floor joist plenum spaces were 0.305 m wide, 0.356 m deep, and 1.83 m long. The wall stud spaces were 0.368 m wide, 0.076 m deep, and 1.83 m tall. The plenum spaces then fed into return duct network that had a C/S area 0.356 m × 0.203 m.

External ventilation and leakage losses from the structure was characterized by performing leakage test in accordance to ASTM E779 [15]. During this air-tightness test, the HVAC system was in passive state (air flow through the duct was still allowed) and all the interior doors were open. Leakage of the entire structure was determined to be 8.3 air changes per hour at 50 Pa (ACPH50). This ACPH50 value correspond to a moderately tight house, which lies in between a typical single-story house having 10 ACPH50 and a tight house having 2 ACPH50 [16]. An equivalent leakage area was estimated as 0.137 m^{-2}, defined as the area of a sharp-edged hole that would create the same leakage flowrate as the building would if both were subjected to a gauge pressure of 10 Pa. When the HVAC system was on (fan was active and no fire), the flowrates at each supply and exhaust vent were measured using a flow hood measurement system [17] before the first experiment. The flowrates were verified to remain the same during the experimental series. These measurements were later utilized for optimizing the flowrates through the simulated HVAC system.

3. Simulation Setup

The simulations were conducted using FDS v. 6.7.9, an open source software developed and maintained by National Institute of Standards and Technology (NIST), that solves Navier–Stokes equations for low-Mach number (Ma < 0.3), fire-driven flows [18]. The default sub-grid turbulence model (Deardorff model) and single-step mixing controlled combustion of the fuel was used for all these simulations. The fuel was defined as a mixture of 92.5 vol.% propane, 5 vol.% propylene, and 2.5 vol.% butane with carbon monoxide yield of 0.0057 and soot yield of 0.028, determined by assuming contribution corresponding to the volume fraction of the constituent gas to the respective yields [19].

3.1. Structure Setup

To model the full-scale experiments in this study, CAD drawings of the structure were used to create the geometry in FDS. The structure was built in FDS to replicate the experimental setup as closely as possible. The material properties used for building the structure, namely density (ρ), thermal conductivity (k), and specific heat capacity (C_p), are provided in Table 2.

The basement floor was made up of 25.4 cm, thick concrete. The basement's walls were modeled as 61.0 cm thick concrete (outside), 12.7 cm thick insulation and 1.27 cm thick gypsum (inside). The basement's ceiling (and first-floor's floor) was modeled as 1.27 cm thick gypsum (exposed), 29.2 cm thick air-gap, 1.91 cm

Table 2
List of Materials and Thermo-Physical Properties Used in FDS Simulations

Materials	References	ρ (kgm^{-3})	k (Wm^{-1}K^{-1})	C_p (Jkg^{-1}K^{-1})
Concrete	[20]	2400	1.6	750
Insulation	[21, 22]	20	0.04	700
Gypsum	[20]	960	0.17	1100
Air-gap	[22]	1	0.03	1000
Wood	[23]	652	0.13	1200
Cement-board	[22, 24]	925	0.18	1000
Glass	[22]	2500	1.4	840

thick oriented strand board (OSB), and 1.27 cm thick cement-board (inside) respectively. The stairs were modeled as 1.27 cm thick cement-board (exposed) and 3.8 cm thick OSB (inside). The first floor exterior walls were modeled as 0.63 cm thick cement-board (outside), 1.1 cm thick OSB, 9 cm thick air-gap, and 1.27 cm thick gypsum (inside). All interior walls were modeled as 1.27 cm thick gypsum, 9 cm thick air-gap, and 1.27 cm thick gypsum. All windows were double pane, and thus simulated as 0.4 cm thick glass, 1 cm thick air-gap, and 0.4 cm thick glass. The three basement windows and the basement door on the side of the burner (Side D) were sealed tightly with cement-board during the experiments and thus, these were simulated to have zero leakage along with an additional layer of 1.9 cm thick cement-board on the inside. All doors, except for the front door, were modeled as 0.4 cm thick OSB, 3.8 cm thick air-gap, and 0.4 cm thick OSB. Front door was simulated as 3.8 cm thick OSB.

For the fire size considered here, $\dot{Q} = 300$ kW, the characteristic fire diameter (D*), evaluated using properties of air at 293 K, is estimated to be 67 cm. The cubic cell dimension (Δx) was defined to be either 5 cm, 10 cm, or 20 cm, which correspond to D*/Δx ratio of 13.6, 6.7, and 3.4 respectively for the 300 kW fire. The results of the mesh dependence study are shown in the Appendix A, following which the cell dimension was defined as 10 cm for all the final simulations.

3.2. HVAC System Setup

The HVAC duct network, reliant on the specification of nodes, duct, and vents in FDS, was built by closely following the actual HVAC duct network, as shown in Fig. 2. The supply and return vents in the structure were placed at the as-built locations, creating nodes in the HVAC duct network. Ducts were placed to connect the supply or return vent node with the node that was located at the next duct intersection. The simulated network layout for the structure is shown in Fig. 13. The ducts were made of galvanized steel and the surface roughness was assumed to be negligible (1×10^{-5} m). The ducts were assigned areas corresponding to the cross sectional area of the duct. In each duct the loss coefficients for forward and backward flow were assigned the same values. The loss coefficients were initialized based on ASHRAE Handbook for Fundamentals [25] and the

geometry of each duct. The loss coefficients at supply and return vents were systematically changed until the vent flowrates agreed with the experimental cold-flow (without any fire) measurements. The optimization process is discussed briefly in Appendix B, where the final cold-flow vent flowrates through the simulated HVAC duct network are compared with the measured cold-flow vent flowrates.The final optimized loss coefficient for each duct is provided in Table 3.

The leaks from the residential structure to the ambient were described using two approaches—(a) assigning local leakage for each window and door, b) assigning zones in FDS with leakage area and leakage surfaces. In both approaches, the estimated equivalent leakage area of 0.137 m^2 to the ambient (Sect. 2) was distributed across the structure. In the first approach, localized leakages were assigned along the top and bottom edge of each exterior door or window. Each door or window was assigned a total leakage given by the estimated equivalent leakage area multiplied by the ratio of that door/window perimeter to the total perimeter of all doors and windows. Half of the leakage was assigned at the top of the door/window, and the other half to the bottom. In the second approach, the perimeter based leakage areas were assigned as pressure zone leakage areas. The equivalent leakage area estimated for all closed rooms (such as bedroom 3 and bedroom 1 in these four experiments) was 7.3×10^{-3} m^2, which was assigned to the external windows in these rooms. For both approaches, basement windows and the door near the fire (Side D), which were sealed with gypsum board during the experiments, were also modeled as completely sealed and therefore these openings were not used for distributing the leakage area throughout the structure. Open area under the closed doors (about 0.9 m wide) was estimated to be about of 0.01 m^2 (about 0.0127 m gap height). Therefore, leaks under the doors (for local leakage and zone leakage approach) were simulated with a leak area of 0.01 m^2.

The HVAC fan, for the experiments when it was on, was simulated using a fan curve. The manufacturer-provided fan curve was fit with a second-order polynomial function such that the flowrate at 0 Pa was 0.60 m^3 s^{-1}, at 20 Pa was 0.59 m^3 s^{-1}, at 100 Pa was 0.54 m^3 s^{-1}, and at 600 Pa was 0 m^3 s^{-1}. When the HVAC was off, the volume flowrate induced by the fan was forced to be 0 m^3 s^{-1}. HVAC filter, which was replaced with a new one for each experiment, was added to the furnace node of the HVAC model with an initial loss coefficient of 11, no initial soot deposition, and a linear increase in loss coefficient by a value of 1 for every gram of soot filtration. The filter was simulated to have a fixed efficiency of 85%. The ambient temperature used in the simulations were approximated as the average temperature determined from the baseline data for each experiments. The ambient temperatures was between 20°C and 27°C for these four experiments. Simulations were then conducted to model the experiments shown in Table 1. The gas burner ramp simulated in all experiments was a 1 s rise to the steady-state HRR at 5 s into the simulation. The simulations were run until 60 s after the fuel supply to the burner was shutoff. It is important to note that the objective of this study was to compare the predicted steady-state environment with the experimental data and therefore, fire-growth was not the focus of the modeling. To facilitate quantitative comparison of measurements and FDS predictions, steady-state data was defined as the state of the system when rate of change of measured differen-

tial pressure was negligible and all sensors had responded to the fire-induced environment. Although temperatures and gas concentrations did not reach a constant value when the burner fuel was shut-off, all the sensors had responded to the fire-induced environment by that time. Thus, average values of quantities during the last 60 s before the fuel shut-off was chosen as a 'steady-state' approximation for comparing FDS predictions with measurements.

4. Results

The experiments with the HVAC on (Ba2 and Ba4) had an experimental duration of approximately 450 s and the experiments with HVAC off (Ba1 and Ba2) had a duration of 900 s. The shorter duration for the experiments with HVAC on was limited by the clogging of the HVAC filter to avoid potential damage to the compressor unit of the HVAC system.

Figure 3 shows a representative predicted temperature contour at 1.8 m above the floor for the basement and first-floor for experiment Ba2. As expected, the highest temperatures are in proximity of the burner in the basement. The transport of combustion products is evident by the temperature distribution throughout the structure. The temperatures decrease away from the fire as the hot combustion products travel towards the stairwell and to the first floor. While the lowest temperatures are seen in the closed bedroom 3, the transport of combustion products through the HVAC duct network can be seen in this room, where the temperature near the supply vent is slightly higher than anywhere else in this room.

In the subsequent sections, profiles of the measured and the predicted quantities were compared for one basement location, bedroom 2, and bedroom 3. The basement location provides a reasonable location to compare measured and predicted fire-induced environment around the burner. The open (bedroom 2) and closed (bedroom 3) rooms are representative rooms to compare the transport of gases inside these rooms by either buoyancy-driven or HVAC-driven flow.
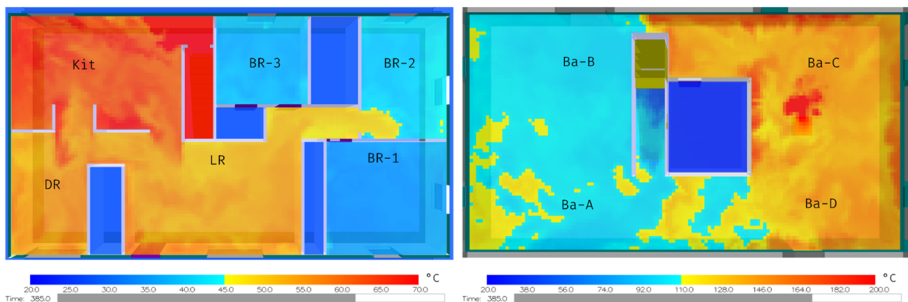

Figure 3.   Predicted temperature distribution at 1.8 m above the floor for the first floor (left) and the basement (right) for experiment Ba2 (HVAC on, door open). The annotations refer to approximate locations of the thermocouple trees.

4.1. Fire-Induced Pressure

The fire-induced pressure development in the residential structure is compared with FDS predictions at 1.22 m above the floor for A/B basement quadrant, bedroom 2, and bedroom 3 in Fig. 4. These plots show experimental and FDS data processed by taking a 5 s moving average. The error bars shown for the experimental data represent the expanded uncertainty of 20% and additional 1 Pa calibration uncertainty as a result of the device noise. In these plots, comparison is also done for the predictions of pressure by using zone leakage vs. local leakage approach in FDS. The steady-state pressure predicted by both leakage approaches is similar, but the peak pressure is consistently higher for the simulations using localized leakages. FDS predicted the general pressure development—the pressure on the first floor being slightly positive while the pressure in the basement being slightly negative. Such behavior is reasonable from the stand-point of a buoyancy-driven flow—the hot combustion gases rise up to the first floor and leak out to the ambient, and a slightly negative pressure in the basement allows makeup air to enter the basement and sustain the fire.

FDS predicted local steady pressure change with height qualitatively well compared with the experiments—a higher pressure closer to the ceiling than that closer to the floor, as shown in Fig. 15 in Appendix C. Steady-state pressure in A/B quadrant at 0.3 m and 2.13 m above the floor was measured to be ~ -2 Pa and ~ 2 Pa respectively. FDS predicted the steady-state pressure of ~ -7 Pa and ~ -2 Pa at these locations, respectively. Similar trend in steady-state and peak pressure predictions was observed for simulations of tests with the HVAC on, Ba2 (door open) and Ba4 (door closed). The approach of prescribing local leakages provided better peak pressure magnitude prediction away from the fire-room while zone leakage approach provides better peak pressure magnitude prediction for the fire-room. The measured peak pressure for the basement could be lower due to the much larger volume of the basement (about 210 m^3) compared to the volume of a single bedroom (between 20 m^3 and 35 m^3). Thus, further comparison of gas species and temperature development was done only for simulations that utilized local leakage approach. It is also important to note that the equiva-
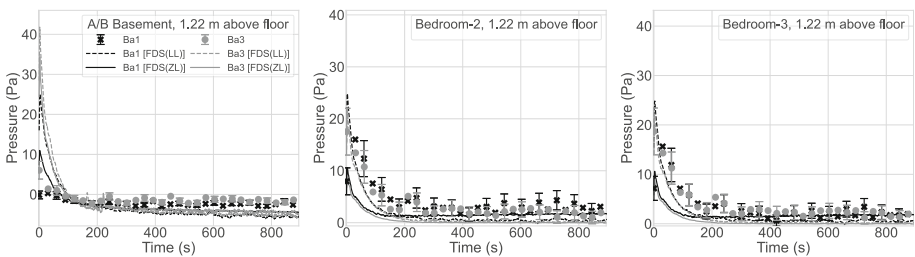

Figure 4. Measured differential pressure compared with FDS predictions, made using local leakage (LL) and zone leakage (ZL) approaches, for experiments Ba1 (HVAC off, door open) and Ba3 (HVAC off, door closed).
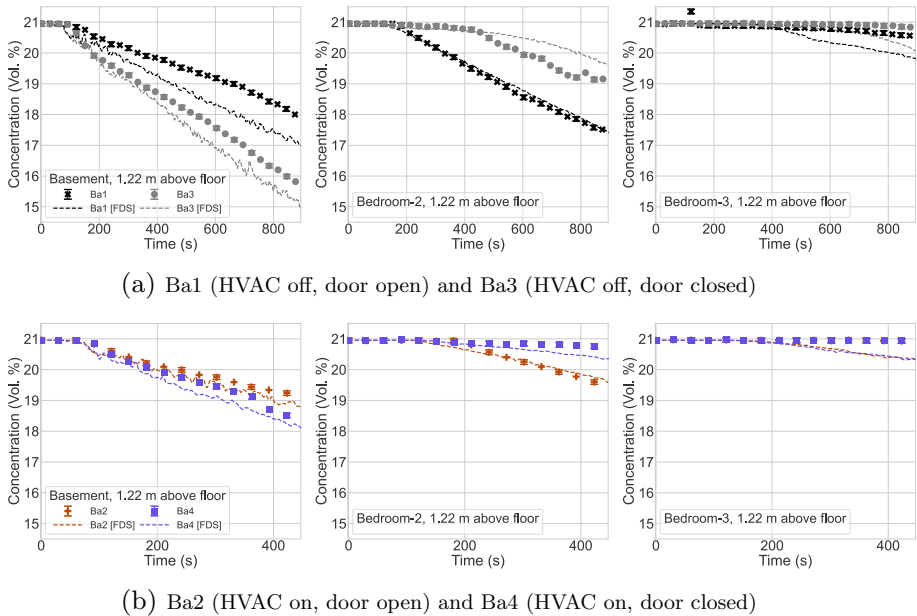
(a) Ba1 (HVAC off, door open) and Ba3 (HVAC off, door closed)

(b) Ba2 (HVAC on, door open) and Ba4 (HVAC on, door closed)

Figure 5. Profiles of measured volumetric oxygen content compared with FDS predictions.

lent leakage area, estimated experimentally using ASTM E779, have uncertainties associated with it. The sensitivity of FDS predictions to the assumed interior door leakage and the total exterior leakage and its distribution was not examined in this study and should be investigated in the future.

4.2. Gas Species

Temporal profiles of oxygen concentration measured at 1.22 m above the floor in terms of vol.% for the four experiments are shown in Fig. 5. The error bars shown for the experimental data represent the expanded uncertainty of 12% and a 0.05 vol.% calibration uncertainty as a result of the device noise. For the measured locations, total vol.% decrease in oxygen was highest in the basement (fire-room), followed by the open bedroom (bedroom 2) and then the closed bedroom (bedroom 3). Qualitatively, the predicted trend of reduction in volumetric oxygen content is similar to that observed in the experiments. The steady-state volumetric oxygen content in the basement reaches around 18 vol.% (at about 850 s) for the experiment with open stairwell door and HVAC off (Ba1) and around 15.8 vol.% for the experiment with closed stairwell door and HVAC off (Ba3). At the same locations and time, FDS predicted the concentrations to be about 17 vol.% and 15 vol.% respectively, which correspond to about 6% and 5% respective over-prediction in reduction of volumetric oxygen content from the initial conditions. FDS predicted the steady-state concentration in the basement when the HVAC is on similar to that observed in the experiments (around 19 vol.% for Ba2 and 18 vol.% for Ba4). FDS prediction of the steady-state oxygen content reduction in

the open bedroom (bedroom 2) is similar to that of the experimental measurements in this room for all four scenarios. FDS slightly over-predicted the reduction in oxygen content at steady-state condition in the closed bedroom (bedroom 3) for all four scenarios, possibly a consequence of over-prediction in gas transport which might be partially due to leakage assumptions.

Temporal profiles of carbon dioxide and water vapor concentration measured at 1.22 m above the floor in terms of vol.% for the four experiments are shown in Figs. 6 and 7. The error bars shown for the experimental data for carbon dioxide represent the expanded uncertainty of 12% and a 0.3 vol.% calibration uncertainty as a result of the device noise. The error bars shown for the experimental data for water vapor represent the expanded uncertainty of 10% and a 0.2 vol.% calibration uncertainty as a result of the device noise. The production of these two species in the basement follows approximately a linear growth to steady-state values that are higher for CO_2 production and lower for H_2O production than the measured values. CO_2 concentration in the open bedroom (bedroom 2) is higher when the HVAC is off (Ba1 and Ba3) than when HVAC is on (Ba2 and Ba4). This trend is predicted by FDS. This is a result of adding fresh (or fresher air) to the bedroom through the supply vent. Steady-state H_2O and CO_2 concentration in the closed bedroom (bedroom 3) is predicted within 1% of the measured value.

(a) Carbon dioxide content
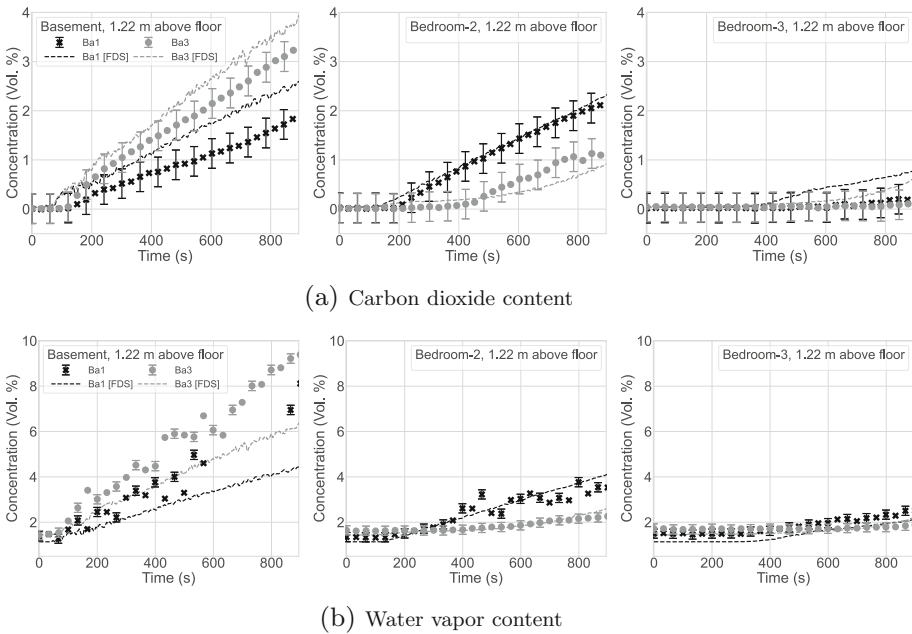

(b) Water vapor content

Figure 6. Profiles of measured carbon dioxide and water vapor concentrations compared with FDS predictions for experiments Ba1 (HVAC off, door closed) and Ba3 (HVAC off, door closed).
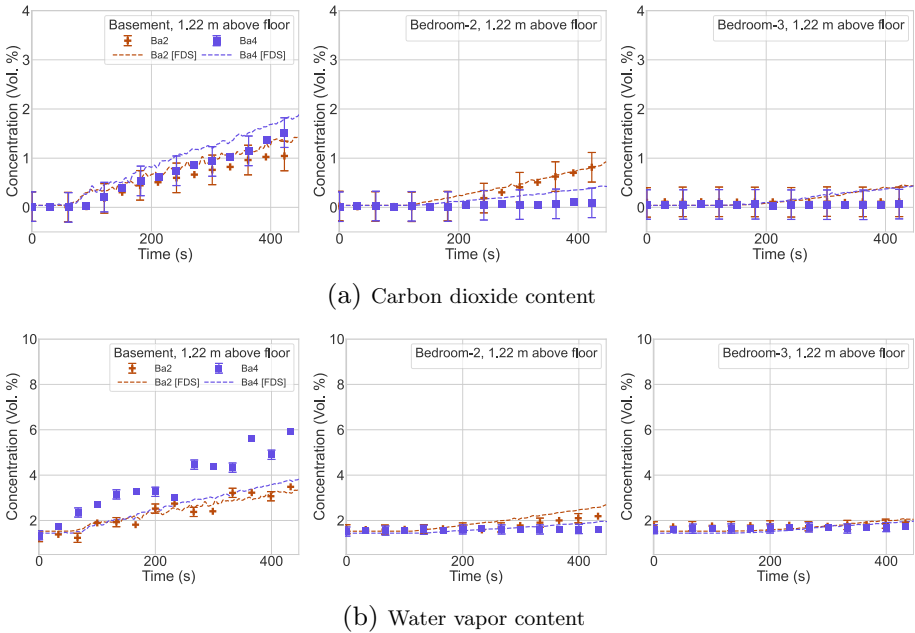
(a) Carbon dioxide content

(b) Water vapor content

Figure 7. **Profiles of measured carbon dioxide and water vapor concentrations compared with FDS predictions for experiments Ba2 (HVAC on, door open) and Ba4 (HVAC on, door closed).**

4.3. Temperature

Temporal profiles of temperature at 2.13 m above the floor in the basement (fireroom), bedroom 2 (open door) and bedroom 3 (closed door) are shown in Fig. 8 for the four experiments. Error bars shown for all the experimental temperature data represent expanded uncertainty of 5%, as discussed in Sect. 2.1. The temperature predictions shown here are from the FDS thermocouple devices and the uncorrected thermocouple data from the experiments. In all of these plots, time t = 0 s corresponds to the ignition of the burner fuel. The data are shown approximately until the burner fuel supply was cutoff. The measured steady-state temperature as a function of height for these three locations across all four experiments are compared with the predicted data in Fig. 16 in Appendix C.

The temperature in the lower left location in Fig. 2 also labeled as Ba-A in Fig. 3 at 2.13 m above the floor reaches around 170°C and 140°C in experiments Ba1 and Ba3, respectively, and around 150°C and 125°C in experiments Ba2 and Ba4, respectively. FDS under-predicted this steady-state temperature value by about 30°C for the case where the stairwell door is closed (Ba3 and Ba4) and by about 10°C when HVAC is off (Ba1 and Ba2). Under-prediction of steady-state temperature could be attributed to uncertainties in leakage flows and heat losses to the walls (which include predictive errors in heat transfer and uncertainty in wall thermophysical properties). Future experiments should consider measuring heat fluxes to the walls, ceilings, and floors and wall surface temperatures which
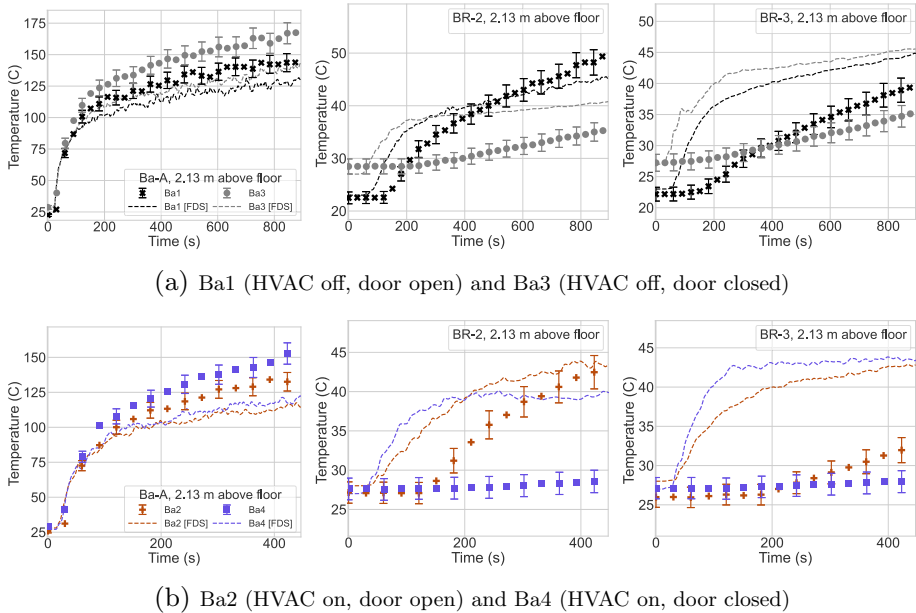
(a) Ba1 (HVAC off, door open) and Ba3 (HVAC off, door closed)

(b) Ba2 (HVAC on, door open) and Ba4 (HVAC on, door closed)

Figure 8.   Profiles of measured temperature change compared with FDS predictions.

could provide valuable information to validate heat losses through the walls and potentially improve temperature predictions.

The difference between the temperature rise in the open bedroom and the temperature rise in the closed bedroom was consistently larger when the stairwell door was open (Ba1 and Ba3) than when the stairwell door was closed (Ba2 and Ba4). This indicates that the dominant mechanism for hot gas transport to the open bedroom (bedroom 2) when the stairwell door is open is via convective transport due to buoyancy-induced transport of hot gases to the first floor. On the other hand, the transport of hot gases to the closed bedroom (bedroom 3) and to the open bedroom when the stairwell door is closed (Ba3 and Ba4) is predominantly via the HVAC duct network. The dominance of these mechanisms for transport to bedrooms 2 and 3 was confirmed by comparing the predicted volumetric flowrate into each of these rooms from all possible pathways.

Despite the prediction of dominant gas transport pathways to individual rooms, the temperature increase when the transport is dominated via the HVAC duct network is over-predicted by FDS by about 10°C to 15°C. This could be the consequence of not considering heat losses from the HVAC duct to the ambient, which could be important especially considering the fact that the HVAC duct network supplying to the first floor was designed to traverse through the roof and other parts of the structure without being directly affected by hot combustion products.

To confirm whether the removal of heat from an HVAC duct compensates for the over-prediction of the temperature in the closed bedroom-3, additional simulation was conducted for experiments Ba2 and Ba4 with a feature to remove heat
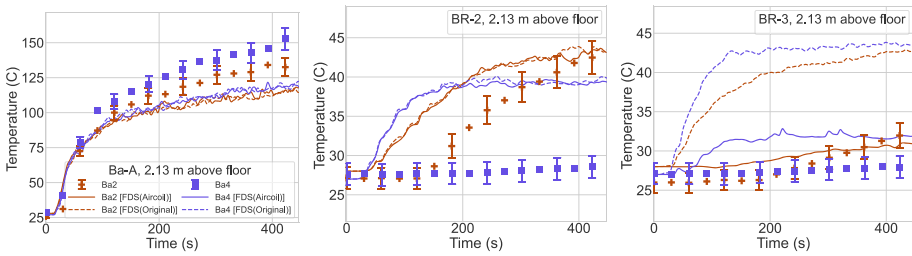
Figure 9. Effect of including HVAC duct heat loss to the duct feeding into bedroom 3 on temperature predictions.

from the duct supplying air to bedroom 3 (Duct S-13). The air flow predicted into bedroom 3 from the supply vent S-13 was at a rate of 0.03 $m^3 s^{-1}$ and temperature of 80°C. An FDS Aircoil device was added to this duct to remove heat at a fixed rate, simulated as a linear rise from 0 kW to the heat loss value in 5 s. After performing simulations with different heat loss rates, the fixed heat loss rate of 1.5 kW provided temperature predictions in the room that agreed with experimental data. The prediction of temperature in bedroom 3 for experiments Ba2 and Ba4 for simulations with 1.5 kW steady heat loss is compared with the original simulation in Fig. 9. After consideration of heat loss from the duct, the steady-state temperature rise in the closed bedroom is similar to the experimental steady-state values for both the experiments. The predictions of steady-state temperatures in the open bedroom (bedroom 2) and the basement A location are unaffected by the addition of the heat loss only to the duct that feeds to the vent S-13 in bedroom 3, as expected. From this figure, including heat loss from the duct that feeds into bedroom 3 improved the predictions of temperature rise in this room, indicating the need to include heat loss to the ambient from a non-insulated HVAC duct network.

Assuming the duct loses heat with the ambient air and considering the duct as a cylindrical heat exchanger, the internal heat transfer coefficient is estimated to be 9.8 $W\,m^{-2}\,K^{-1}$ for the predicted FDS flowrate using Dittus–Boelter equation for cooling [22]. Assuming the ambient air is steady at 20°C and that the external heat transfer coefficient is somewhere between 5 $W\,m^{-2}\,K^{-1}$ and 10 $W\,m^{-2}\,K^{-1}$ (estimated from correlations of natural flow for a cylinder in cross-flow and parallel-flow [22]), the temperature drop observed in the air entering bedroom 3 corresponding to 1.5 kW heat loss rate is estimated to occur in 3.8 m to 4.8 m of the duct (perimeter ∼1 m) length. This length corresponds approximately to the non-insulated section of the duct network that passes from the HVAC room through bedroom 3 closet to the attic space. Although the duct network in the attic-space was insulated, some heat loss from the duct to the ambient may be occurring in attic too. Since calculation of steady-state rate of heat loss requires knowledge of temperature drop, the heat loss estimated here is a reasonable adjustment to the FDS predictions rather than a prediction itself. A general approach can be intro-

duced in the FDS to account for heat losses from the HVAC duct by estimating convective heat loss to the ambient from a non-insulated duct section.

4.4. Steady-State Temperature

The steady-state data predicted by the FDS model (original simulations without the HVAC duct heat loss) for different regions of the residential structure are compared with the experimental data in Fig. 10. As discussed in Sect. 2.2, the steady-state data was approximated by averaging 60 s of data prior to the burner fuel shutoff. The data in this figure illustrate two basement fires (experiments Ba1 and Ba2). This figure shows the steady-state average temperature of the thermocouple array, peak temperature of the thermocouple array, linear rise rate to the peak temperature, and average time to observe a 10% change in temperature in the different regions of the structure (refer to TC annotations in Fig. 3). From this
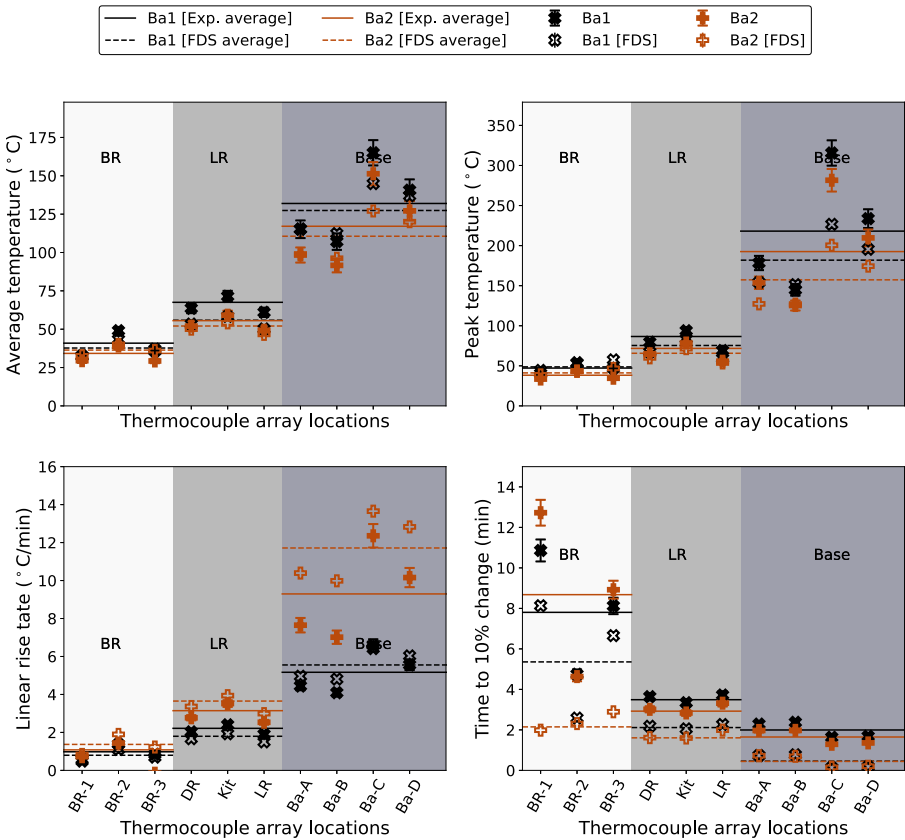

Figure 10. Comparison of predicted and measured steady-state temperatures for basement fires. x-axis label with BR = Bedroom followed by the number of the bedroom, DR = Dining-room, Kit = Kitchen, LR = Living-room, Ba = Basement followed by respective quadrant as shown in Figs. 2b and 3.

figure, it can be seen that the average and peak experimental temperature values (filled symbols) for the experiment with HVAC off (Ba1) are higher than those for the experiment with HVAC on (Ba2). FDS predictions of the peak and average temperature (open symbols) also show similar behavior for these two experiments. The average steady-state temperatures at all locations throughout the structure were found to be statistically different (Wilcoxon signed-rank test, p-value < 0.01) for experiments with and without the HVAC on, regardless of the door position, for both experimental and FDS predicted data.

The total rise in temperature is smaller when HVAC is on, possibly due to the extraction and re-circulation of hot combustion products and replenishment with cooler air from the supply vents. The rate of linear increase of temperature is faster and the time at which 10% change in temperature is observed is sooner (especially away from the basement fire-room) when HVAC is on than when HVAC is off. Similar trends were also observed when the stairwell door was closed (experiments Ba3 and Ba4).

4.5. *Statistical Comparison*

To facilitate quantitative comparison of FDS predictions and measured values of steady-state conditions (temperature and gas species), a scatter plot of FDS predictions and experimental data is shown in Fig. 11 for the basement fire experiments compared here (Table 1). The data in these plots are the steady-state values, obtained by averaging the last 60 s of the data (for both experiment and FDS) before the burner fuel was shutoff. The temperature and oxygen scatter charts are plotted by considering the change in the respective quantity from the initial condition. Data where the temperature change was less than $0.4°C$, oxygen concentration reduction was less than 0.2%, volumetric water vapor concentration was below 0.2%, and volumetric carbon dioxide concentration was below 0.5% were neglected in these plots and accumulating statistics. These threshold values approximately correspond to maximum uncertainty of the collected data for the respective measurement.

The statistics of model prediction and experimental data, shown in these plots, were calculated by following the guides to quantify the model uncertainty [26, 27]. In these scatter plots, a model bias factor of 1 indicates predictions which match with the experimental data (ideal). A value lower than 1 indicates an under-prediction and a value above 1 indicates an over-prediction. The solid black line indicates the expected perfect agreement between the predicted values and the experimental data. The solid red line passes through the distribution mean and indicates the expectation line multiplied by the bias factor. The solid dashed line indicates the expanded experimental uncertainty, and the red dashed lines indicate the model uncertainty, calculated as two standard deviations of the scatter in the bias factor.

The change in temperature is predicted reasonably well when the change is less than about $100°C$ and is under-predicted for higher temperature change. Overall, the FDS under-predicted temperature, indicated by the model bias factor of 0.91. FDS temperature predictions also have a larger scatter-model uncertainty (total
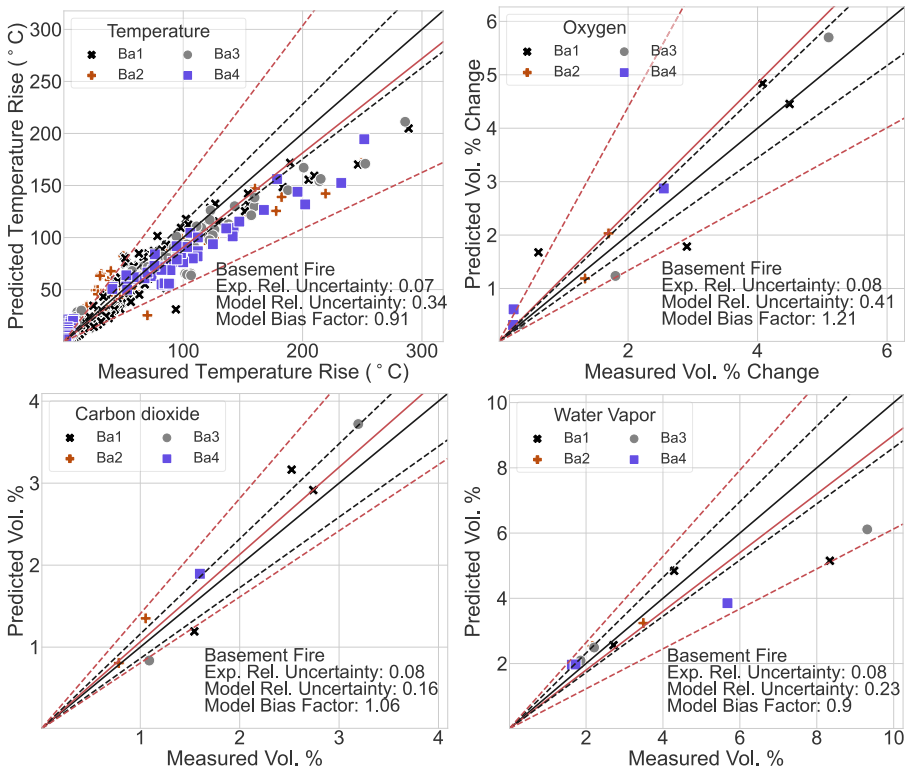
Figure 11. Comparison of measured and predicted temperature rise, volumetric oxygen change, water vapor, and carbon dioxide content (in clockwise direction from top-left) for experiments Ba1 through Ba4.

expanded uncertainty with coverage factor of 2) of 0.34 vs. experimental uncertainty of 0.07. This means that the temperature change was under-predicted by 9% ± 34% on average. A similar plot obtained for the hot gas layer (HGL), assumed as temperature measurement at 2.4 m above the floor, indicated a bias factor of 0.98 and a model relative uncertainty of 0.44. The bias factor of HGL prediction in the previous FDS validation exercise for forced ventilation was 1.12 with a relative uncertainty of 0.15 [26]. The bias factor calculated for the current work is lower compared to previous validation efforts, and a larger scatter in predicted data is observed in the current work.

The change in volumetric oxygen content was over-predicted (model bias factor of 1.21) and has higher scatter (relative uncertainty of 0.41) than that of the experimental data (relative uncertainty of 0.08). Volumetric carbon dioxide content was generally over-predicted (model bias factor of 1.06) and also has a larger scatter (relative uncertainty of 0.16) than the experimental data (relative uncertainty of 0.08). The volumetric water vapor content was predicted well until

4 vol.% but under-predicted at higher volumetric content. The overall bias factor of the FDS model for water vapor prediction was 0.9 and the predictions have a larger scatter (relative uncertainty of 0.23) than that of the experimental data (relative uncertainty of 0.08). It is noted that the number of gas measurement locations was much less than the number of temperature measurement locations. As a result, the certainty in the gas prediction statistical quantities is lower than for the temperatures.

5. Conclusion

This study conducted validation of FDS 6.7.9 for controlled fire in a full-scale residential structure with an HVAC system. In this study, data from experiments performed in a purpose-built two-story, moderately air-tight residential house was utilized to understand the capability of the FDS to predict the effect of natural and forced ventilation on fire-induced environment. The HVAC system, with a 10.55 kW cooling capacity and a volumetric flowrate capacity of up to 2040 m^3 h^{-1}, was typical to the Pennsylvania region where the experiments were conducted. The ventilation parameters studied here were the HVAC status (on vs. off) and door position (open vs. closed) for a gas burner fueled fire in a basement location. Differential pressure, temperature, and volumetric content of oxygen, carbon dioxide and water vapor were measured in the experiments to facilitate comparison with the simulation results.

The experimental data of equivalent leakage area, obtained from air-tightness test, was utilized to distribute leakage across the structure in proportion to the perimeter fraction of windows and doors. The measured cold-flow HVAC vent flowrates (without fire) were used to optimize the loss coefficients of the HVAC duct network. The steady-state prediction of differential pressure in the fire-induced environment was found to be comparable when the leakages were described either by pressure zones or by local leak paths. Both approaches, however, under-predicted the steady-state pressures, but peak pressure was better captured when describing leakages via local leak paths. Generally, FDS predicted the pressure distribution throughout the structure similar to that observed in the experiments, with a slightly higher pressure on the first-floor and a slightly negative pressure in the basement. A higher pressure was also predicted at higher elevation as compared to the lower elevation at any location in the structure.

The transport of gas species to the open bedroom was predicted correctly to be dominated by convective transport driven by buoyancy-induced flow to the first-floor while the transport to the closed bedroom was predicted correctly to be dominated by transport through the HVAC duct network. Steady-state oxygen and carbon dioxide content was over-predicted (higher consumption of oxygen) and water vapor content was under-predicted, especially in the fire-room.

For all experimental scenarios considered here, it was concluded that the steady-state temperature distribution (both measured and predicted) throughout the structure was statistically different when HVAC was on versus when HVAC was off, regardless of the stairwell door position. Temperature rise in the rooms

away from the fire-room when the HVAC was on was measured and predicted to occur sooner, at a faster linear-rise rate than when the HVAC was off. However, the measured total rise in temperature inside and outside the fire-room was lower when the HVAC was on versus when the HVAC was off. Closed doors were most effective in terms of inhibiting the transport of gases.

FDS over-predicted the total temperature rise to the closed room where the gas transport primarily occurred via the HVAC duct network. Including heat loss from the duct feeding into this room, estimated as sensible enthalpy responsible for the over-predicted temperature rise, was shown to improve the total temperature rise prediction in this room. A more comprehensive methodology can be employed in FDS to include the heat loss in the HVAC duct network, via calculation of average heat transfer coefficient and estimating the effective temperature drop for the length of a duct, to improve the temperature predictions of the air supplied through the HVAC duct network. On average, FDS under-predicted temperatures and water vapor content by about 9% and 10% respectively and over-predicted carbon dioxide and oxygen content by about 6% and 21% respectively. FDS simulations could be improved by higher accuracy of parameters such as HRR, properties of the wall components, and initial conditions of the experiments. Additionally, measurements such as heat fluxes to the wall and surface temperature of walls, ceilings, floors would help quantify and validate heat losses through the walls. The sensitivity of the predictions to leakage area and distributions should also be investigated in future. It is important to note that although FDS development is a continuous process, present models in FDS provide predictions with reasonable accuracy of the fire-induced environment in a residential structure with an HVAC system.

Acknowledgements

Author Contributions

DMC: Formal analysis, Data curation, Investigation, Validation, Visualization, Writing—original draft, Writing—review & editing. CW: Conceptualization, Data curation, Funding acquisition, Methodology, Resources, Supervision, Writing—review & editing. JEF: Methodology, Software, Writing—review & editing.

Funding

Data Availability

Available on request.

Code Availability

Not applicable.

Declarations

Conflict of interest The authors declare that they have no conflict of interest.

Open Access

Appendix A: Mesh Dependence Study

Simulation of the experiment Ba2 was performed with a uniform mesh having cubic cell dimension of either 5 cm, 10 cm or 20 cm. The comparison of the temperature prediction with the experimental data is shown in Fig. 12. In the simulation which used the 5 cm cell size, the 5 cm cell size was prescribed only in the basement around the region of the fire—from the HVAC-room wall to the interior wall of the basement. The cubic cells of dimension (Δx) 5 cm, 10 cm and 20 cm correspond to the $D^*/\Delta x$ ratio of 13.6, 6.7, and 3.4 respectively. The steady-state temperatures obtained for the mesh size of 5 cm and 10 cm are similar and the volumetric oxygen content is predicted closer to the experimental data,

especially for the fire-room (basement). Therefore, simulations presented earlier were conducted using 10 cm cubic cells.

Appendix B: Cold Flow HVAC Vent Flowrates

The FDS HVAC solver models HVAC systems as a network of nodes (where the system connects to computational domain or an internal connection between two or more ducts) and ducts (where a duct connects two nodes and may contain multiple HVAC components such as multiple straight lengths and elbows). Figure 13 shows the HVAC network as modeled in FDS, and Table 3 provides the duct length, duct cross-sectional area, and connected nodes (positive flow is 'from node' towards 'to node'). Measurements of the flowrate from all the supply and return vents were made multiple times during the experimental series. An air flow cone [17] was placed over each vent with the HVAC system running and all interior doors open. The average values of these measurements were then targeted in the cold flow simulation for optimizing minor loss coefficients of the duct network. ASHRAE 2017 Fundamentals' handbook [25] was utilized to obtain preliminary loss coefficients. A 90° elbow with long radius, short radius, or a mitered corner were assigned loss coefficient of 0.6, 0.9, or 1.3 respectively. Airflow through a duct or a tee was assessed to have loss coefficient of 0.5 if the flow
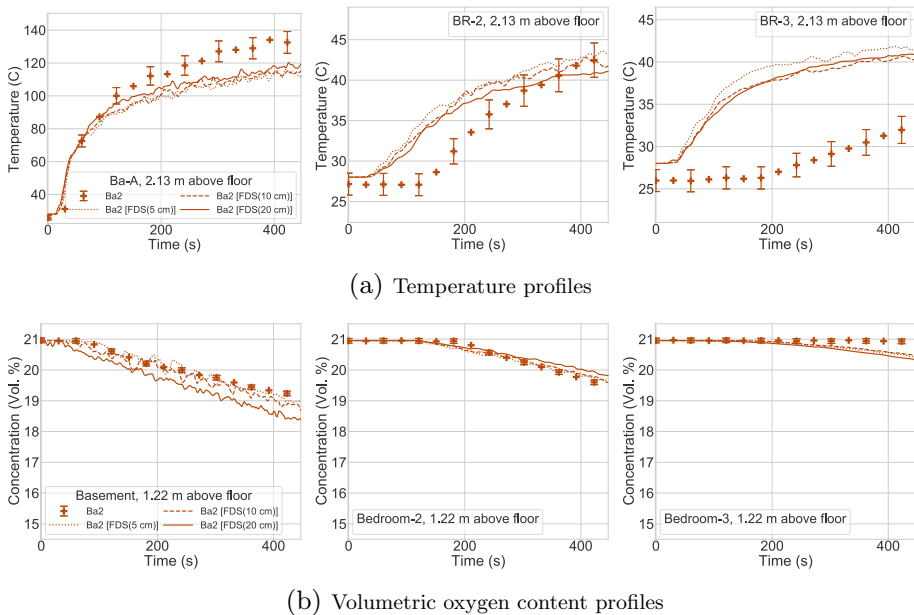

(a) Temperature profiles

(b) Volumetric oxygen content profiles

Figure 12. **Profiles of measured temperature and volumetric oxygen content compared with experiment Ba2 FDS simulation performed by using uniform mesh having cubic cells of dimension of either 5 cm, 10 cm, or 20 cm.**
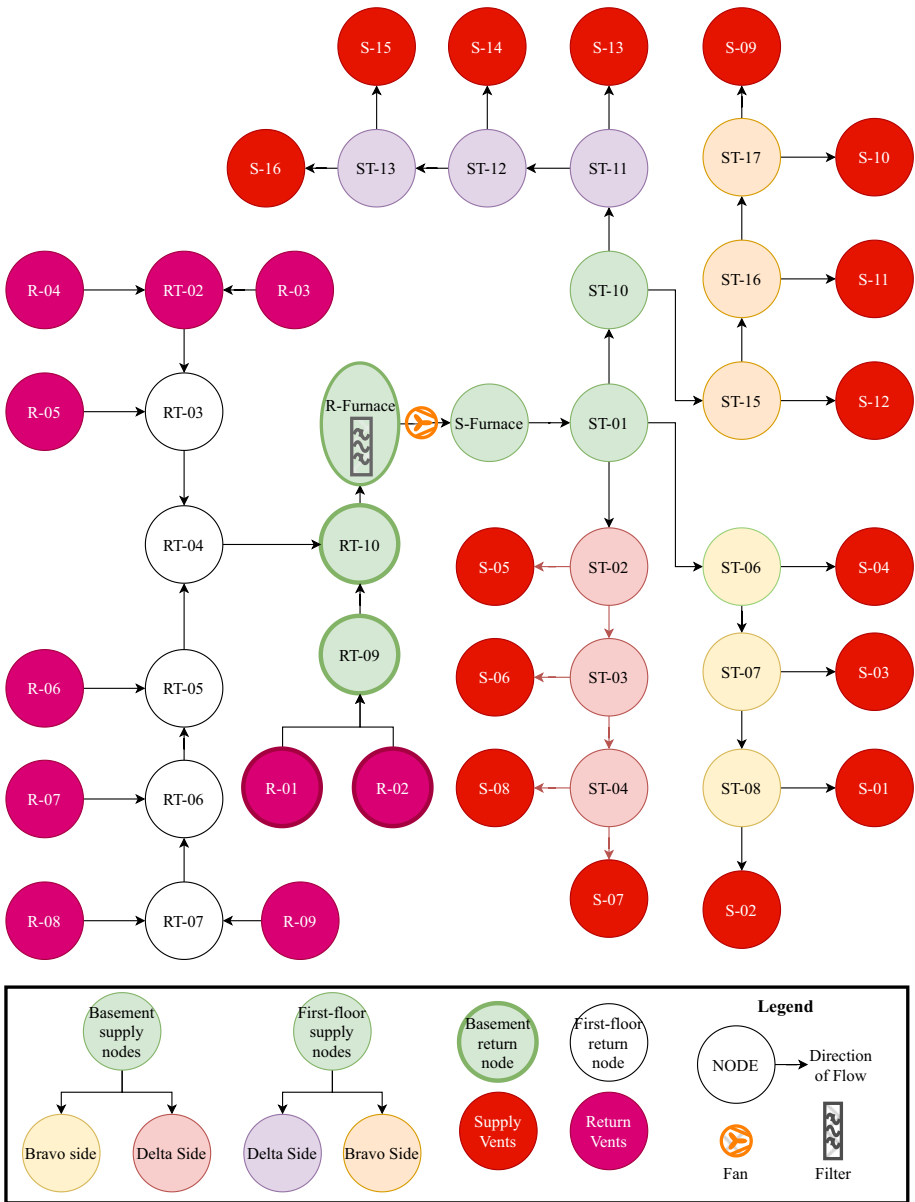
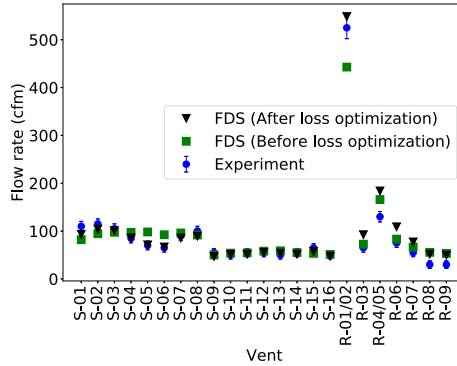**Figure 13. Schematic of network layout of the modeled HVAC system.**

Figure 14. Comparison of measured and predicted HVAC vent flowrate for cold flow (without fire) case, before and after optimization.

Table 3
Details of Nodes, Lengths of the Duct Connecting the Nodes, Cross-Sectional Area, and Final Optimized Loss Coefficients

From node	To node	Length (m)	Area (m²)	Loss coefficient
R-Furnace	S-Furnace	1.0	0.2000	1.3
S-Furnace	ST-01	0.2	0.2000	0.0
ST-01	ST-10	3.0	0.0720	2.3
ST-01	ST-06	5.6	0.0720	2.2
ST-06	S-04	5.6	0.0248	5.1
ST-06	ST-07	0.4	0.0720	0.5
ST-07	S-03	1.2	0.0248	3.6
ST-07	ST-08	2.4	0.0720	0.5
ST-08	S-02	1.2	0.0248	3.1
ST-08	S-01	6.4	0.0248	3.1
ST-01	ST-02	1.4	0.0720	3.9
ST-02	S-05	2.2	0.0248	8.0
ST-02	ST-03	0.4	0.0720	0.5
ST-03	S-06	3.0	0.0248	8.0
ST-03	ST-04	0.8	0.0720	1.1
ST-04	S-07	3.4	0.0248	4.1
ST-04	S-08	1.8	0.0248	4.1
ST-10	ST-11	0.8	0.0600	1.8
ST-11	S-13	2.8	0.0180	4.1
ST-11	ST-12	0.6	0.0600	0.5
ST-12	S-14	3.8	0.0180	3.6
ST-12	ST-13	3.4	0.0600	0.5
ST-13	S-16	3.0	0.0180	4.1
ST-13	S-15	3.8	0.0180	2.6
ST-10	ST-15	2.6	0.0600	1.8

Table 3
continued

From node	To node	Length (m)	Area (m²)	Loss coefficient
ST-15	S-12	2.8	0.0180	3.6
ST-15	ST-16	0.4	0.0600	0.5
ST-16	S-11	3.8	0.0180	3.6
ST-16	ST-17	0.4	0.0600	0.5
ST-17	S-09	3.8	0.0180	4.1
ST-17	S-10	2.8	0.0180	3.6
R-03	RT-02	4.6	0.0620	5.4
R-04	RT-02	2.2	0.0620	6.4
RT-02	RT-03	0.4	0.0720	0.5
R-05	RT-03	2.2	0.0620	6.4
RT-03	RT-04	3.4	0.0720	2.8
RT-05	RT-04	0.4	0.0720	2.8
R-06	RT-05	2.4	0.0620	4.9
RT-06	RT-05	0.8	0.0720	1.0
R-07	RT-06	3.0	0.0620	4.9
RT-07	RT-06	4.2	0.0720	3.0
R-08	RT-07	2.2	0.0620	4.9
R-09	RT-07	2.2	0.0620	5.4
RT-04	RT-10	1.6	0.1290	1.4
R-02	RT-09	0.2	0.0620	3.4
R-01	RT-09	0.2	0.0620	2.4
RT-09	RT-10	0.4	0.1000	0.8
RT-10	R-Furnace	0.6	0.1290	0.9

direction did not change, and 1.8 if the direction changed through the duct section. The initial guess for the loss coefficient at each vent grille was assumed to be 4, regardless of whether the vent was a supply or a return vent. As mentioned in Sect. 2.2, loss due to duct surface reference was assumed to be negligible compared to losses due to elbows and other duct fittings. Forward and reverse losses were assumed to be equal. The loss coefficients for supply and exhaust vents were adjusted in an iterative process such that the differences between the FDS vent
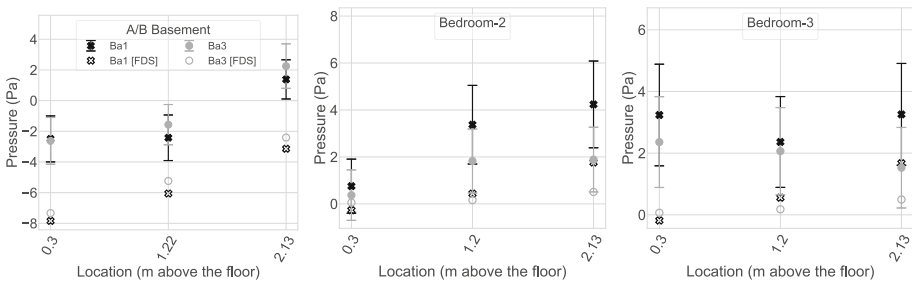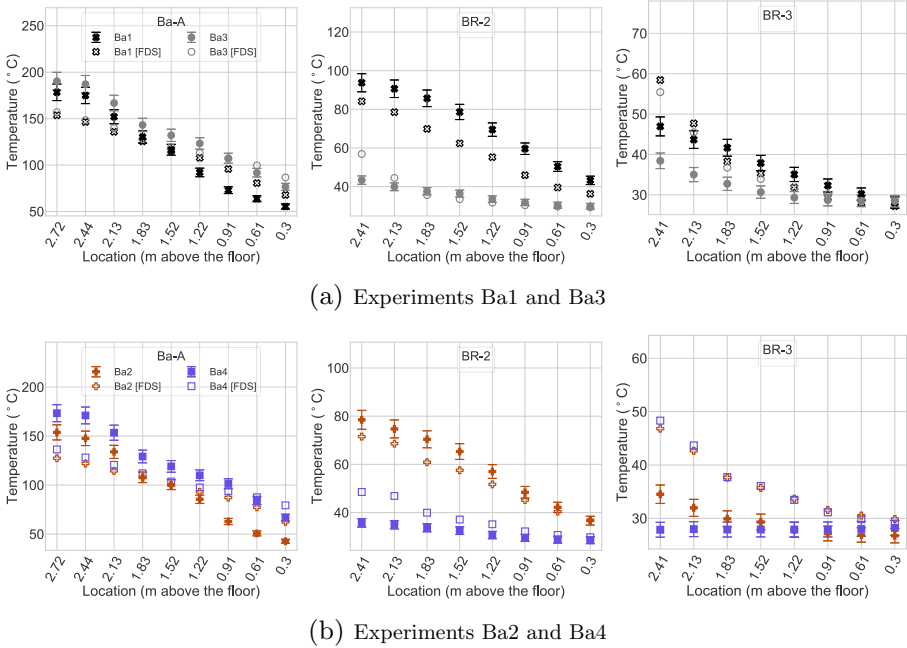

Figure 15. Steady-state pressure predictions for simulations using local leakage approach compared with measurements.

(a) Experiments Ba1 and Ba3

(b) Experiments Ba2 and Ba4

Figure 16. Steady-state temperature predictions compared with measurements.

flowrates and the experimental vent flowrates reached an acceptable value. The final loss coefficients are also tabulated in Table 3. The final flowrates predicted by FDS are shown in Fig. 14. The errors shown here are the reported error of the device, which was 3% of measured volume and a additional 7 $ft^3\,min^{-1}$ (cfm) systematic uncertainty [17]. The reason why higher discrepancy is observed between the predicted and measured return flowrates could not be identified and requires further investigation.

Appendix C: Steady-State Quantities as a Function of Height

The steady-state data was calculated as a 60 s average of the data before the burner fuel was shutoff in the experiments. For experiments Ba1 (HVAC off, door open) and Ba3 (HVAC off, door closed), this time duration was approximately 800 s to 860 s. For experiments Ba2 (HVAC on, door open) and Ba4 (HVAC on, door closed), this time duration was approximately 400 s to 460 s (Figs. 15, 16).

References

1. USFA-FEMA: civilian fire fatalities in residential buildings (2017–2019). Topical Fire Report Series 21(3) (2021)
2. Hostikka S, Janardhan RK, Riaz U, Sikanen T (2017) Fire-induced pressure and smoke spreading in mechanically ventilated buildings with air-tight envelopes. Fire Saf J 91:380–388. https://doi.org/10.1016/j.firesaf.2017.04.006
3. Brohez S, Caravita I (2020) Fire induced pressure in airthigh houses: experiments and FDS validation. Fire Saf J 114:103008. https://doi.org/10.1016/j.firesaf.2020.103008
4. Ghanekar S, Weinschenk C, Horn GP, Stakes K, Kesler RM, Lee T (2022) Effects of HVAC on combustion-gas transport in residential structures. Fire Saf J 128:103534. https://doi.org/10.1016/j.firesaf.2022.103534
5. Klote JH (1999) CFD simulations of the effects of HVAC-induced flows on smoke detector response. ASHRAE Trans 105 (January), Chicago, Illinois, U.S.A, pp 395–409
6. Floyd J (2011) Coupling a network HVAC model to a computational fluid dynamics model using large eddy simulation. Fire Saf Sci . https://doi.org/10.3801/IAFSS.FSS.10-459
7. Ralph B, Carvel R (2018) Coupled hybrid modelling in fire safety engineering; a literature review. Fire Saf J 100(February):157–170. https://doi.org/10.1016/j.firesaf.2018.08.008
8. Ralph B, Carvel R, Floyd J (2019) Coupled hybrid modelling within the Fire Dynamics Simulator: transient transport and mass storage. J Build Perform Simul 12(5):685–699. https://doi.org/10.1080/19401493.2019.1608304
9. Humphries LL, Beeny BA, Gelbard F, Louie DL, Phillips J (2017) MELCOR computer code manuals. Technical Report Janurary, U.S. Nuclear Regulatory Commission, Washington D.C
10. Audouin L, Rigollet L, Prétrel H, Le Saux W, Röwekamp M (2013) OECD PRISME project: fires in confined and ventilated nuclear-type multi-compartments—overview and main experimental results. Fire Saf J 62(PART B):80–101. https://doi.org/10.1016/j.firesaf.2013.07.008
11. Wahlqvist J, Van Hees P (2013) Validation of FDS for large-scale well-confined mechanically ventilated fire scenarios with emphasis on predicting ventilation system behavior. Fire Saf J 62(PART B):102–114. https://doi.org/10.1016/j.firesaf.2013.07.007
12. Quiat A (2020) Analysis of propane gas burner experiments and FDS simulations in a two-story residential structure with HVAC. PhD Thesis, University of Maryland, College Park
13. Weinschenk C, Ghanekar S, Stakes K, Quiat A, Kesslar RM, Lee T (2023) Gas burner experiments conducted in residential structure with HVAC system. Data in Brief 46 (February). https://doi.org/10.1016/j.dib.2022.108825
14. Pitts WM, Braun E, Peacock RD, Mitler HE, Johnsson EL, Reneke PA, Blevins LG (2002) Temperature uncertainties for bare-bead and aspirated thermocouple measurements in fire environments. Therm Meas Found Fire Stand ASTM STP 1427:3–15. https://doi.org/10.1520/stp10945s
15. ASTM International (2019) Standard test method for determining air leakage rate by fan pressurization. ASTM International, West Conshohocken. 10.1520/E0779-19
16. Persily AK (1998) Airtightness of commercial and institutional buildings: blowing holes in the myth of tight buildings. Thermal Envelopes VII Conference (December), Clearwater, Florida, U.S.A, pp 829–837
17. Testo 420 flow hood system—UX-30009-52. https://www.coleparmer.com/p/testo-420-flow-hood-system/72876. Accessed 15 Mar 2023

18. McGrattan KB, Hostikka S, Floyd J, McDermott R, Vanella M (2021) Fire dynamics simulator user's guide. Technical report. National Institute of Standards and Technology, Gaithersburg. https://doi.org/10.6028/NIST.SP.1019, https://nvlpubs.nist.gov/nistpubs/Legacy/SP/nistspecialpublication1019.pdf

19. Tewarson A (2008) Generation of heat and chemical compounds in fires, Table 3.4.16. In: DiNenno PJ, Drysdale D, Beyler CL, Walton WD, Custer RLP, Hall JR Jr. and Watts JM Jr., SFPE handbook of fire protection engineering, 4th ed., pp 3-105–3-194

20. Salley M, Wachowiak R (2012) Nuclear power plant fire modeling application guide (NPP FIRE MAG) NUREG-1934, vol November 2012, p 305

21. R-13 EcoTouch® PINK® FIBERGLAS™ Insulation. https://insulation.owenscorning.com/homeowners/insulation/products/r-13-fiberglas-insulation/ Accessed 13 Apr 2022

22. Bergman TL, Lavine AS, Incropera FP, Dewitt DP (2018) Fundamentals of heat and mass transfer, 8th edn. Wiley, New Jersey, pp. 983–995

23. Gong J, Zhou H, Zhu H, McCoy CG, Stoliarov SI (2021) Development of a pyrolysis model for oriented strand board: part II-thermal transport parameterization and bench-scale validation. J Fire Sci 39(6):477–494. https://doi.org/10.1177/07349041211036651

24. USG Durock®Brand Cement Board Systems Catalog. http://www.usg.com/content/dam/USG_Marketing_Communications/united_states/product_promotional_materials/finished_assets/durock-cement-board-system-guide-en-SA932.pdf Accessed 13 Apr 2022

25. American Society of Heating, R., Air-Conditioning Engineers I (2017) 2017 ASHRAE handbook: fundamentals. American Society of Heating, Refrigerating and Air-Conditioning Engineers, Inc. (ASHRAE), Atlanta, pp 983–995

26. McGrattan KB, Hostikka S, Floyd J, McDermott R, Vanella M (2021) Fire dynamics simulator technical reference guide vol. 3: validation. Technical report. National Institute of Standards and Technology, Gaithersburg. https://doi.org/10.6028/NIST.SP.1018, https://nvlpubs.nist.gov/nistpubs/Legacy/SP/nistspecialpublication1018.pdf

27. Peacock RD, Reneke PA, Davis DW, Jones WW (1999) Quantifying fire model evaluation using functional analysis. Fire Saf J 33(3):167–184. https://doi.org/10.1016/S0379-7112(99)00029-6